Dynamic load test and rapid load test on two large diameter steel pipe piles with double crossed steel ribs inside the pile bottom section

Shihchun Lin[i], Ryogo Morino [ii], Iku Kurogome [iii], Tsuyoshi Miyatsukasa [ii], Kozo Yamashita [iii], Takaaki Mizutani [iv] and Go Kobayashi [v]

i) M. Sc., Engineering Department, Jibanshikenjo Co., Ltd., 1-16-2, Kotobashi, Sumida-ku, Tokyo 130-0022, Japan.

ii) Deputy Director, Section of Port Construction department, Tokyo Port Construction Office, Bureau of Port and Harbor, Tokyo Metropolitan Government, 3-9-56, Konan, Minato-ku, Tokyo 108-0075, Japan.

iii) Senior Staff Member, Section of Port Construction department, Tokyo Port Construction Office, Bureau of Port and Harbor, Tokyo Metropolitan Government, 3-9-56, Konan, Minato-ku, Tokyo 108-0075, Japan.

iv) D. Eng., Head of Foundations Group, Port and Airport Research Institute, 3-1-1, Nagase, Yokosuka, Kanagawa 239-0826, Japan.

v) Section Manager, Instrumentation Department, Jibanshikenjo Co., Ltd., 1-16-2, Kotobashi, Sumida-ku, Tokyo 130-0022, Japan.

ABSTRACT

Tokyo International Cruise Terminal, a four-story passenger ship terminal, was constructed at the Tokyo Bay area in 2020. The terminal building is on the jacket-type pier foundation supported by large-diameter steel pipe piles (SPPs) having an outer diameter (D_o) of 2 m. A very soft sediment exists below the seabed to a depth of about 35 m. The surface soft layer is underlain by a gravel layer of 4 m thick and a mudstone layer having SPT *N*-values greater than 50. In order to estimate an appropriate embedment length of SPP in the gravel layer or the mudstone layer, rapid load tests (RLTs) were carried out on two SPPs having a length of 57 m (Pile 1) or 62 m (Pile 2). For both SPPs, double crossed steel ribs (#-shaped ribs) were welded inside the piles along the bottom 5 m section. Both piles were instrumented with strain gages at 8 levels to obtain axial forces during RLTs. High plugging was observed in both piles.

Keywords: rapid load test, steel pipe pile, plugging, double crossed ribs, dynamic load test

1 INTRODUCTION

Tokyo International Cruise Terminal, a four-story passenger ship terminal, was constructed at the Tokyo Bay area (Fig. 1) and started the operation in 2020. The terminal building is on a jacket-type pier foundation supported by large-diameter steel pipe piles (SPPs) having an outer diameter D_o of 2 m (Fig. 2). There was no experience of the use of such large-diameter SPPs at this site. Hence, rapid load tests (RLTs) were carried out on two test SPPs to estimate plugging efficiency as well as load-displacement relations in 2017.

Double cross steel ribs (#-shaped ribs) were welded inside each test SPP aiming at increasing plugging efficiency. Dynamic load tests (DLTs) and RLTs were carried out on the two test piles having different embedment lengths into a bearing stratum.

This paper presents results of the load tests and discusses the validity of the #-shaped ribs to increase plugging efficiency.

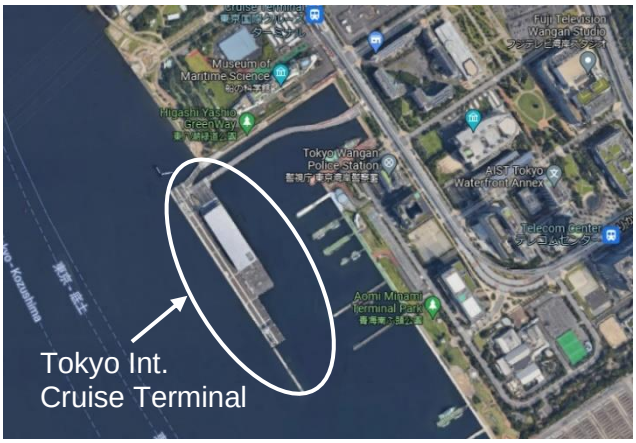

Fig. 1. Location of Tokyo International Cruise Terminal.

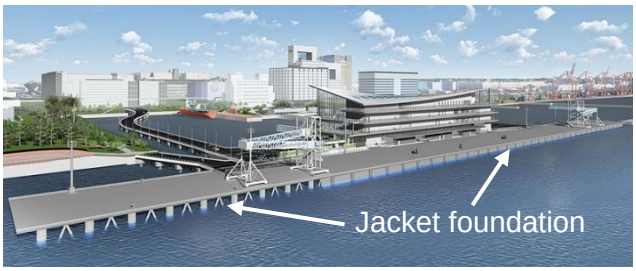

Fig. 2. Jacket foundation for Tokyo International Cruise Terminal.

2 PILE LOAD TESTS

2.1 Site conditions

Profiles of soil layers and SPT *N*-values at two locations of borehole investigations at the site are shown in Fig. 3, together with the final seating of two instrumented test piles designated as Pile 1 and Pile 2. A pre-boring-investigation was conducted 37 m away from the location of Pile 1, while another borehole investigation (designated as Boring P1) was conducted at the same location as Pile 1. Distance between Pile 1 and Pile 2 was 12 m (Fig. 4). The pre-boring was carried in 2016 and Boring P1 was conducted on 25th of March, 2017, only 10 days prior to the driving of the test piles. Hence, the ground conditions from the pre-boring were used for design of the test piles.

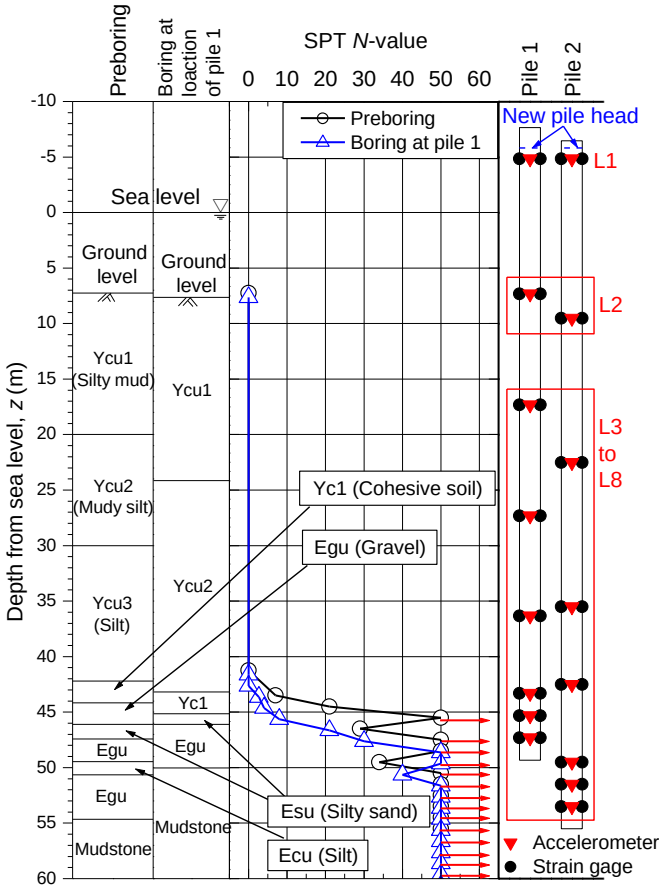

Fig. 3. Profiles of soil layers and SPT *N*-values, together with instrumented test piles.

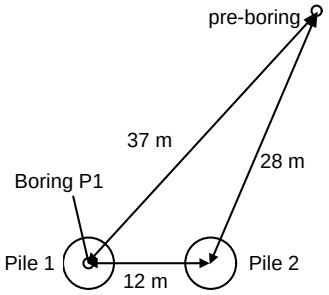

Fig. 4. Locations of boreholes and test piles.

It is seen from both boring investigations that very soft soils ($N \approx 0$) exist from the seabed (depth from the see water level z = 8 m) to a depth z = 42 m. Below the very soft layers exist hard soil layers. However, profiles of SPT *N*-values below z = 42 m are different between both boring locations. A hard bearing layer appears at z = 46 m at the pre-boring location, while it appears at z = 48 m at the location of Boring P1.

2.2 Test piles

Both test piles were made of steel-SKK490. Table 1 shows the specifications of Pile 1 and Pile 2. The only difference between the two test piles was the pile length. Pile 2 was designed to have a greater embedment length into the bearing stratum compared to Pile 1, as shown in Fig. 3. Design load on the pile is 14.26 MN. With a factor of safety F_s = 2.5, the ultimate bearing capacity P_{ult} greater than 35.65 MN is required in the design stage for both piles.

Each pile was instrumented with strain gages and accelerometers at eight levels (L1-L8).

Table 1. Specifications of test piles.

Item	Value	
	Pile 1	Pile 2
Original length, L_o (m)	57.0	62.0
Length after cutting, L_c (m)	55.2	61.4
Outer diameter, D_o (mm)	2000	2000
Inner diameter, D_i (mm)	1952	1952
Wall thickness, t_w (mm)	24	24
Cross-sectional area, A (m^2)	0.1490	0.1490
Young's modulus, E (kPa)	2.10×10^8	2.10×10^8
Density, ρ (ton/m^3)	7.85	7.85
Longitudinal wave velocity, c (m/s)	5172	5172
Design embedment length into bearing stratum, L_{d_des} (m)	2 to 5 ($1D_o$ to $2.5D_o$)	10 ($5D_o$)
Actual embedment length into bearing stratum, L_d (m)	3.2 ($1.6D_o$)	9.4 ($4.7D_o$)
Length of section reinforced by double cross steel ribs, L_r (m)	5.0	5.0
Cross-sectional area of double cross steel ribs, A_r (m^2)	0.1384	0.1384
Mass, m (ton) †	66.66	72.51
Design load (MN)	14.26	14.26
Factor of safety	2.5	2.5
Required ultimate bearing capacity, P_{ult} (MN)	35.65	35.65

†The mass is calculated with original pile length.

Double-crossed steel ribs (#-shaped ribs) were welded inside the piles along a bottom 5 m section as shown in Fig. 5, aiming at increasing plugging effects, in other words, apparent tip resistance. Thickness of the #-shaped ribs was 19 mm.

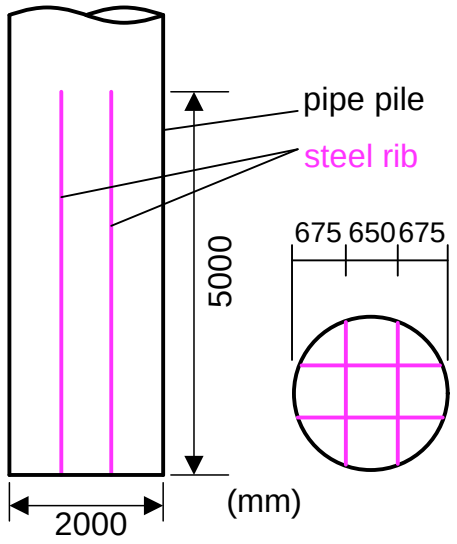

Fig. 5. Steel pipe pile with double crossed steel ribs at the bottom section.

2.3 Test sequences and test results

2.3.1 Test sequences

Installation of Pile 2 was carried out on 4th of April, 2017. Nineteen days after the pile installation, RLTs were carried out. Similarly, installation of Pile 1 was carried out on 5th of April, 2017. Thirty-four days after the pile installation, RLTs were conducted.

During installations of both piles, a vibro-hammer was first used until the pile tip reached the top of the bearing stratum. In reality, the piles were pushed through the upper very soft soils by the self-weights of the pile and the vibro-hammer. After the pile tip reached the bearing stratum, the piles were driven using a hydraulic pile driver IHC S-280. DLTs were carried out during pile driving for drivability study and to grasp "set-up" phenomena of the piles.

2.3.2 Results of DLTs during pile driving

During driving of Piles 1 and 2, set per blow S, rebound R and driving resistance R_d were obtained. The R_d was estimated from the well-known Case method proposed by Rausche et al (1985), using the dynamic signals measured at L1.

As one of objectives in the load tests was comparison of performance of Pile 1 and Pile 2, the test results of the two piles are compared hereafter.

Fig. 6 shows changes of N-value, S, R and R_d with depth z of the pile tip in driving of Pile 2. Pile 2 was driven into the bearing stratum by 9.4 m ($4.7D_o$). S = 2.1 mm/blow, R = 12.3 mm and R_d = 26.4 MN at the final driving. Driving energy at the final driving was 240 kNm.

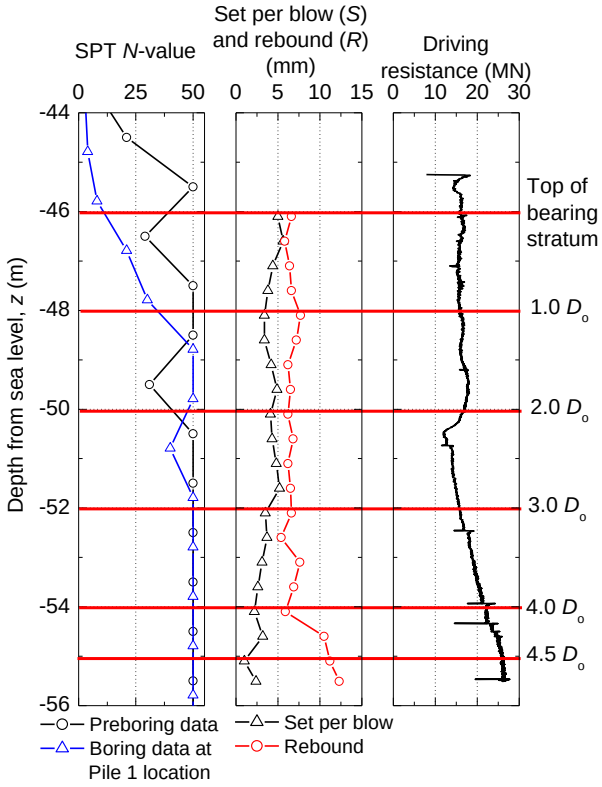

Fig. 6. Dynamic load test results of Pile 2.

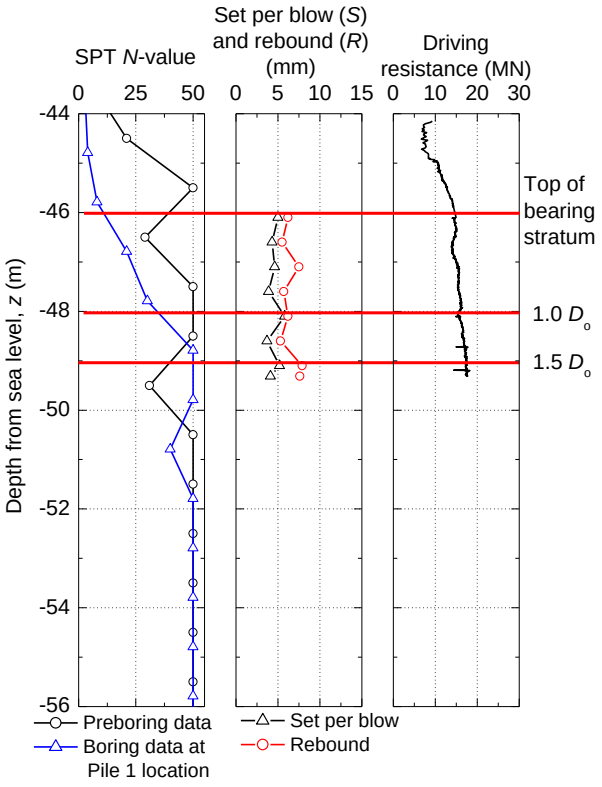

Fig. 7. Dynamic load test results of Pile 1.

Fig. 7 shows the results of DLTs in Pile 1. Pile driving was terminated when the pile tip reached z = 49.2 m. Note here that R_d of Pile 2 started to decrease when the pile tip reached z = 49.5 m and decreased to 12 MN

when the pile tip reached z = 50.4 m, although R_d started to increase again with increasing z. Hence, in case of Pile 1, pile driving was terminated at z = 49.2 m with R_d = 17.5 MN, S = 4.1 mm/blow and R = 7.6 mm. Driving energy at the final driving was 174 kNm.

2.3.3 Results of RLTs

RLTs were carried out using a Hybridnamic device with a hammer mass m_h of 140 ton. A total of 6 blows were applied to Pile 2 with a maximum drop height h = 3.28 m.

To obtain the load-displacement relation at the seabed level (ground level), the dynamic signals measured at L2 were used in the Unloading Point Connection method (ULPC method). The pile length below L2, designated as L_2, was 46 m. For details of the ULPC method, please refer to Kamei et al (2022) or APPENDIX in this paper.

Fig. 8 shows the time histories of rapid loads (F_{rapid}) measured at different pile levels (L1–L8) in the last (6th) blow with h = 3.0 m.

Loading duration t_L at L2 was 99 ms that corresponded to the relative loading duration T_r = $t_L/(2L_2/c)$ = 5.57 where c is the longitudinal stress-wave speed (see Table 1). T_r = 5.57 sufficiently satisfies the criterion for RLT, $T_r \geq 5$, specified in the Japanese code (JGS, 2002).

Similarly, 6 blows were applied to Pile 1. Fig. 9 shows the time histories of F_{rapid} measured at different pile levels (L1–L8) in the last (6th) blow with h = 3.28 m. Loading duration t_L at L2 was 108 ms and L_2 is 42 m, resulting in T_r = 6.65.

It is interesting to note that t_L in Pile 2 is shorter than that in Pile 1, but the maximum value of F_{rapid} in Pile 2 is larger than that in Pile 1, although h in Pile 1 was greater than that in Pile 2. This is reasonable, because Pile 1 reached almost ultimate state during the last blow, as shown below.

Note that the axial forces at L7 and L8 were calculated from the measured strains multiplied by Young's modulus and the cross-sectional area of the pipe section, disregarding the #-shaped ribs.

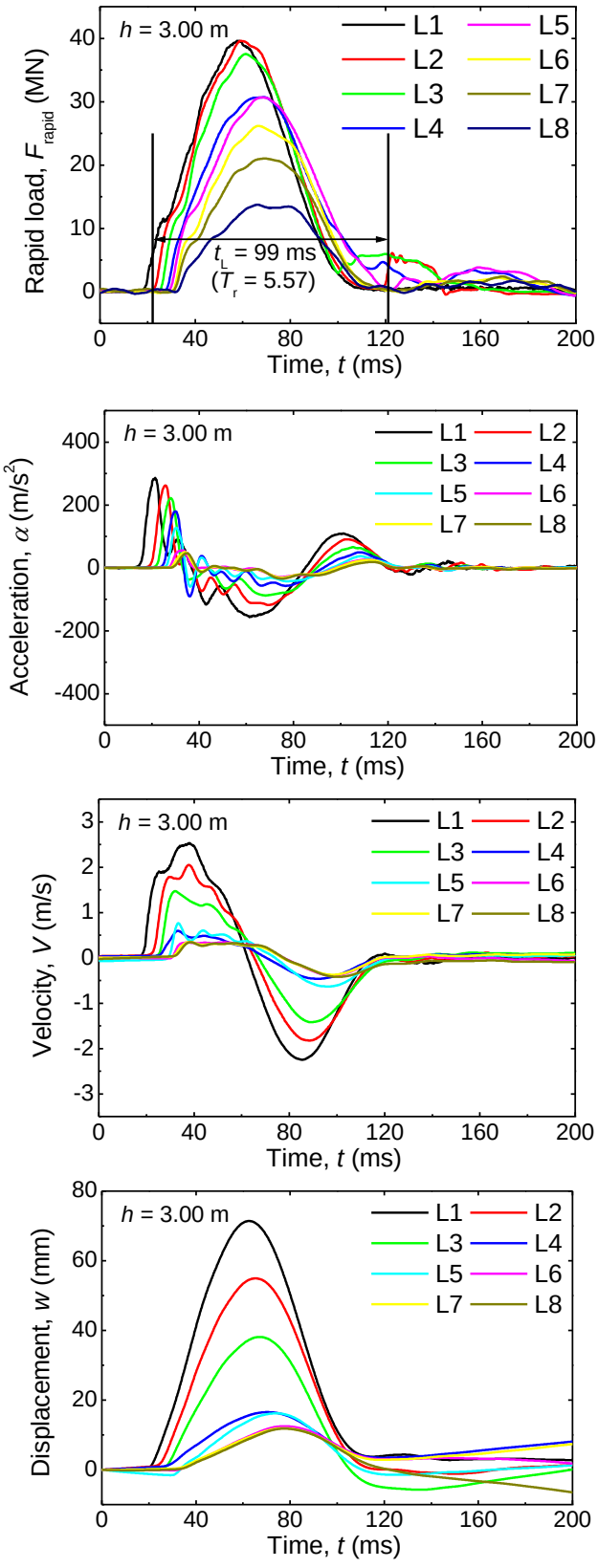

Fig. 8. Measured signals during RLT on Pile 2.

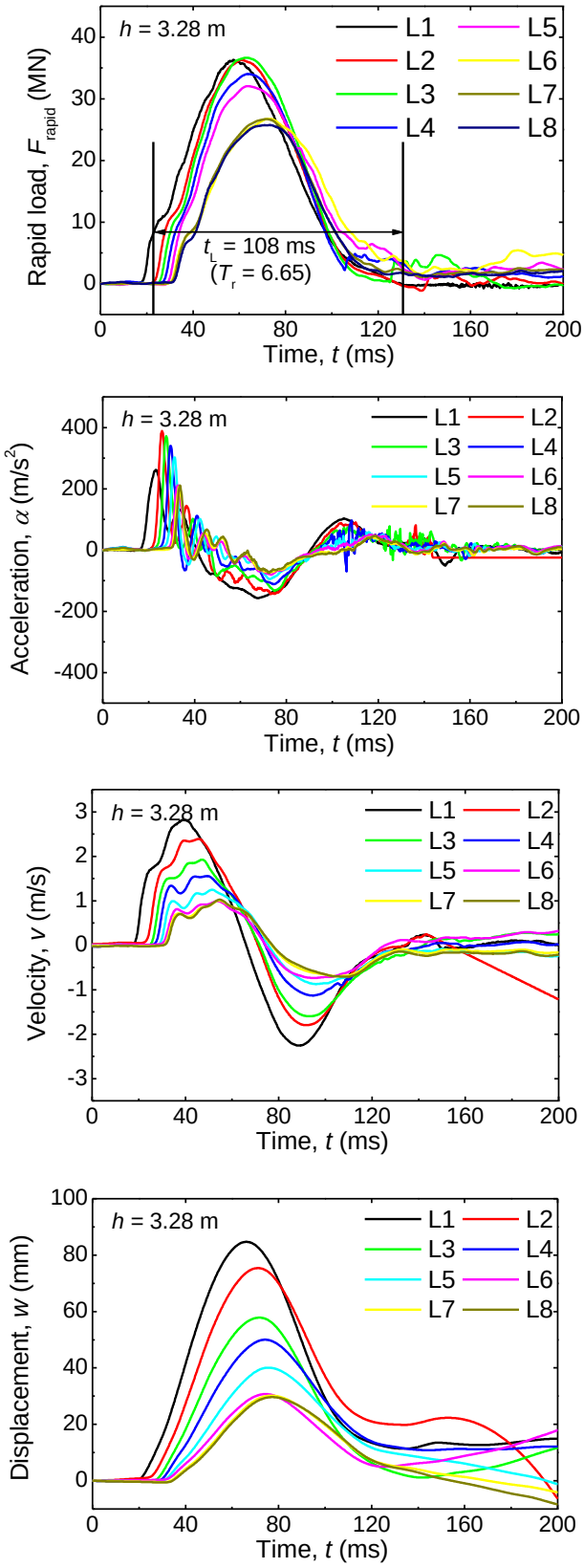

Fig. 9. Measured signals during RLT on Pile 1.

Fig. 10 shows soil resistance R_{soil} vs displacement w of Pile 2 at L2 obtained from RLTs. In this analysis, acceleration measured at L8 was used to avoid overestimation of R_{soil}. When correcting the inertial force of the pile, the inertia force of the soil plug was neglected, because it was difficult to measure the height of the soil plug after pile installation. Neglect of the inertia of the soil plug results in a safer (conservative) value of the pile resistance.

By connecting the Unloading Points (ULPs), the R_{ULP} (static resistance R_w) vs w was constructed. It is clearly seen that although loading to the ultimate state was not achieved, Pile 2 has a static resistance of 40.26 MN at w = 62 mm, which is sufficiently greater than the required ultimate capacity P_{ult} = 35.65 MN.

Shaft resistance is also shown in the figure. This will be explained later.

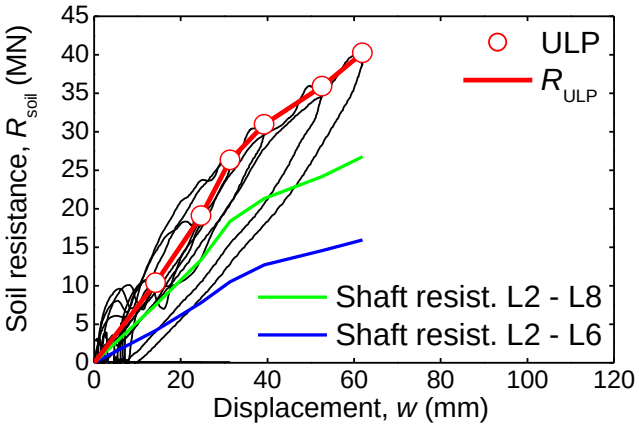

Fig. 10. Result of RLT in case of Pile 2.

Fig. 11 shows the results of RLTs on Pile 1. It is seen that Pile 1 was loaded to nearly ultimate state. P_{ult} = 36.39 MN at w = 93 mm exceeds the required capacity of 35.65 MN.

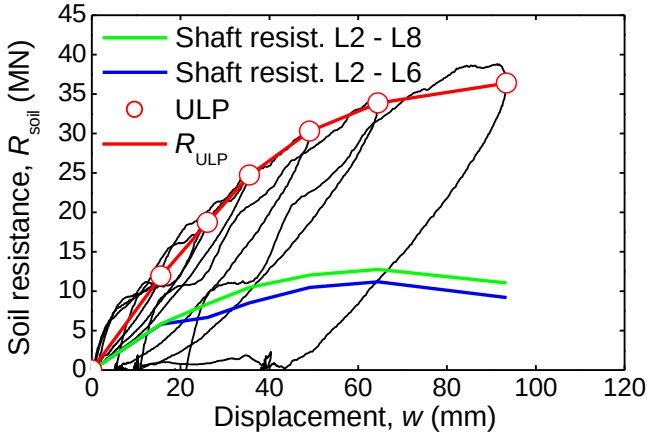

Fig. 11. Result of RLT in case of Pile 1.

As presented in Figs. 6 and 7, the driving resistance R_d of Pile 2 and Pile 1 were 26.4 MN and 17.5 MN, respectively. The maximum static resistance of Pile 2 and Pile 1 were 40.26 MN and 36.39 MN, respectively, showing the so-called "set up" phenomena. Hence, DLT is a very useful tool for criteria for driving termination.

Fig. 12 shows the distributions of axial forces F_a in Pile 2 obtained from RLTs. The F_a were estimated from Eq. (1).

$$F_a(x, t) = F_a'(x, t) - m_x \times \alpha_{L8}(t) \quad (1)$$

where $F_a'(x, t)$ is measured axial force at measurement level L_x of the pile, m_x is mass of pile section below L_x, and $\alpha_{L8}(t)$ is acceleration at L8.

Note that $F_a(x, t)$ at ULP at each measurement level are shown in Fig. 12. ULP is the maximum displacement at each measurement level.

It is seen from Fig. 12 that the soil layer Ycu2 and the pile section between L5 and L8 show relatively large shaft resistance. The shaft resistance almost reaches ultimate state when a pile head load of about 35 MN is applied. On the other hand, the soil resistance below L6 (F_a at L6) and tip resistance (F_a at L8) tend to increase even when the pile head load of 40.26 MN is applied.

Fig. 13 shows the distributions of F_a during RLTs on Pile 1. The shaft resistance reaches the ultimate state when the pile head load attains to about 32 MN. The soil resistance below L6 (F_a at L6) and tip resistance (F_a at L8) tends to increase even when the pile head load reaches 36 MN.

The mobilized shaft resistance in Pile 2 and Pile 1 have been shown in Figs. 10 and 11, respectively. The mobilized shaft resistances were defined as difference of F_a between L2 and L6, and that of F_a between L2 and L8.

Let us compare the unit shaft resistance f_s estimated from RLTs and that used in design.

In Technical Standard and Commentaries for Port and Harbours Facilities in Japan (Ports and Harbours Bureau, 2020), empirical equations (2) and (3) are specified for estimating f_s.

$$f_s = 2N \text{ (kPa) for sandy ground} \quad (2)$$

$$\boldsymbol{f_s} = \begin{cases} \boldsymbol{c_u} & \text{for } \boldsymbol{c_u} \le 100 \text{ kPa} \\ \boldsymbol{100} & \text{for } \boldsymbol{c_u} > 100 \text{ kPa} \end{cases} \quad \text{for clayey ground (3)}$$

where c_u (kPa) is undrained shear strength of surrounding soil.

The values of f_s in each soil layer used in pile design and measured from RLTs are summarized in Table 2 and shown in Fig. 14

f_s of layers Ycu1 and Ycu2 are almost equal between Pile 1 and Pile 2. This indicates a high reliability of RLT. Fig. 14 also shows the simular results between RLTs and empirical values except for the layer of mudstone. It can be said that the empirical equation estimates the f_s reasonably. Also, it shows the importance of implementation of load tests in site for proper design of piles.

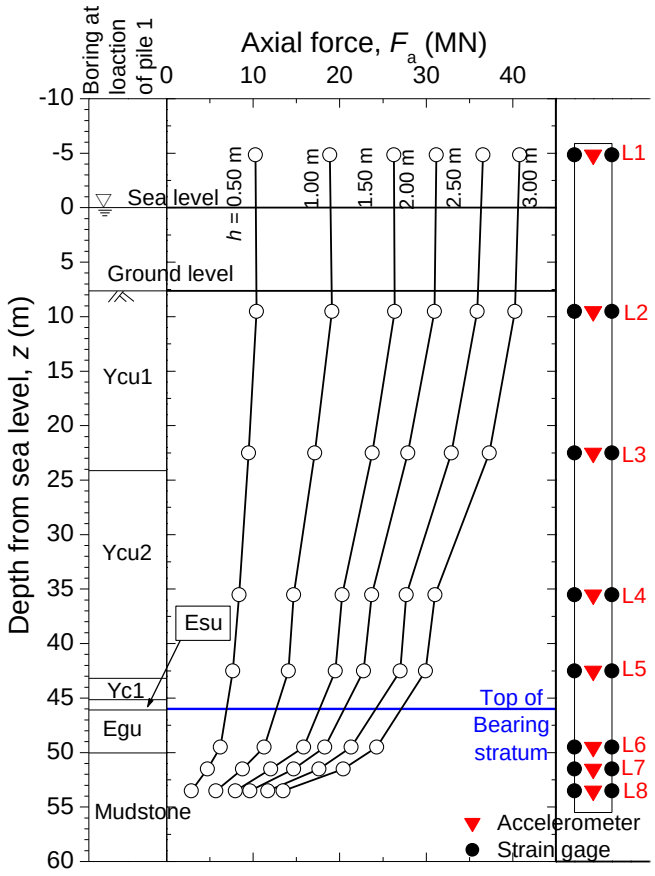

Fig. 12. Distributions of pile axial forces of Pile 2.

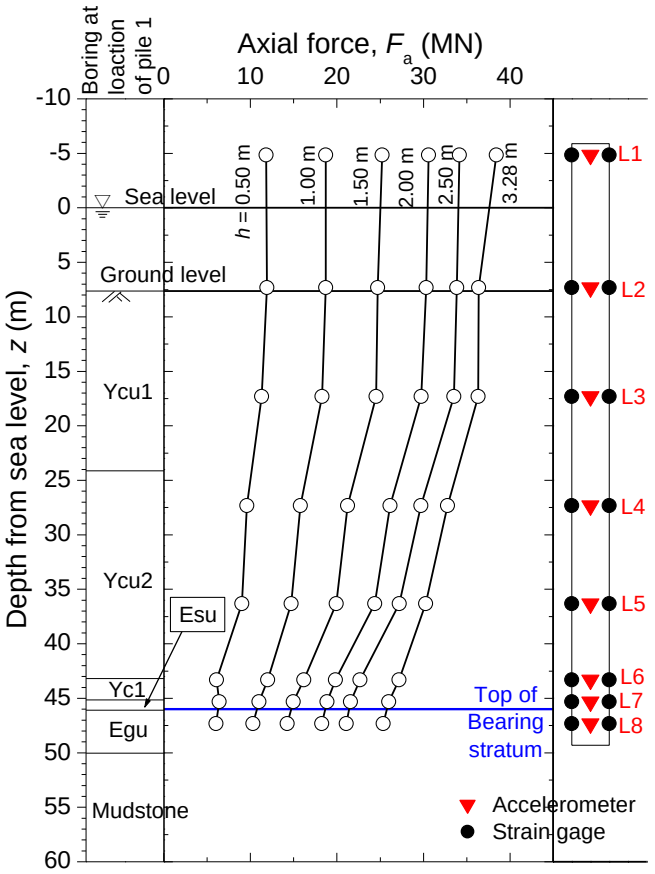

Fig. 13. Distributions of pile axial forces of Pile 1.

Table 2. Unit shaft resistance f_s of the test piles.

Soil layer	Unit shaft resistance, f_s (kPa)			
	Empirical value	Pile 1	Pile 2	Average of Piles 1 and 2
Ycu1(c_u = 48.1 kPa)	48.1	9	38	24
Ycu2(c_u = 63.8 kPa)	63.8	53	51	52
Yc1 (c_u = 100 kPa)	100	104	-	104
Esu (N = 8)	16	99	-	99
Egu (N = 38)	76.0	56	129	98
Mudstone (N = 50)	100	-	431	431

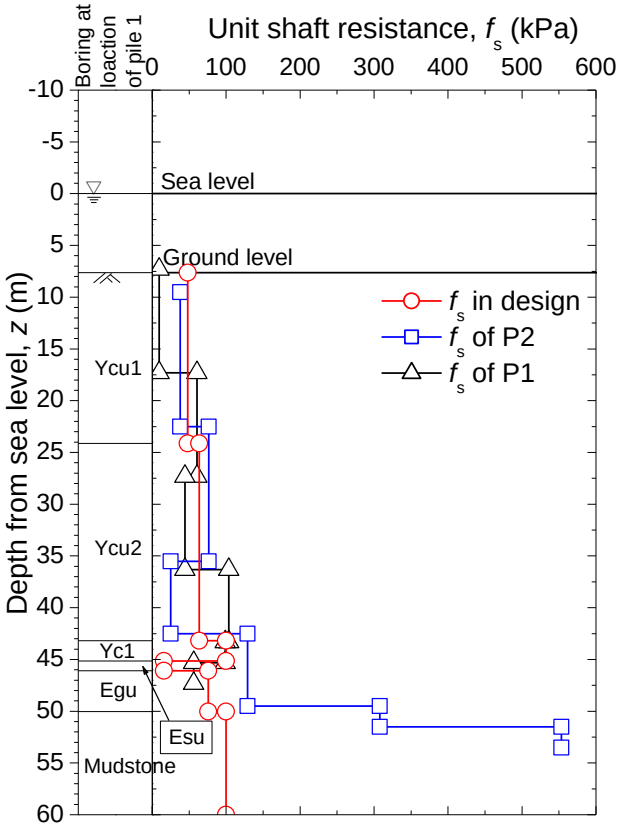

Fig. 14. Unit shaft resistance f_s of the test piles.

2.3.4 Plugging efficiency

Plugging efficiency η is an empirical parameter used to estimate the equivalent unit pile tip resistance q_{d_open} of an open-ended pipe pile compared with that of the close-ended pile (perfectly plugged pipe pile) q_{d_close}. Namely,

$$\eta = q_{d\_open} / q_{d\_close} \quad (4)$$

An empirical equation (5) is specified in Technical Standard and Commentaries for Port and Harbours Facilities in Japan (Ports and Harbours Bureau, 2020).

$$q_{d\_close} = 300N \text{ (kPa)} \quad (5)$$

where N is SPT N-value of the ground around the pile tip calculated as

$$N = (N_1 + N_2) / 2 \quad (6)$$

in which N_1 is SPT N-value of the ground at pile tip and N_2 is mean SPT N-value in the range of $4D_o$ above the pile tip.

N-values of Piles 1 and 2 used in design were 32 and 50, respectively.

In this study, q_{d_open} was estimated from F_a at L8:

$$q_{d\_open} = F_a / (\pi D_o^2/4) \quad (7)$$

Table 3 summarizes the plugging efficiency and the soil resistances estimated from RLTs on Piles 1 and 2.

Plugging efficiency η in Pile 1 is 0.84 despite a shorter embedment length into the bearing stratum. Plugging efficiency η in Pile 2 is 0.29 even though embedment length is larger than that of Pile 1. Please notice that the tip resistance is the minimum estimation because of the conservative calculation as mentioned in Section 2.3.3. The "real" η will be higher than the table show. Also, as mentioned in Fig. 10, ultimate tip resistance was not reached in the load test. It seems that the pile tip resistance would have increased much more if higher load had been applied. Hence, η of Pile 2 is expected to be much greater than 0.29.

Table 3. Plugging efficiency and soil resistance from RLTs.

	Pile 1	Pile 2
Depth of pile tip (m)	-49.32	-55.51
Embedment length into the bearing stratum, L_d (m)	3.22	9.41
Embedment ratio, L_d/D_o	1.6	4.7
SPT N-value of the ground around the pile tip	32	50
Maximum soil resistance, R_{soil} (MN)	36.38	40.26
Shaft friction resistance (MN)	11.05	26.78
Tip resistance (MN)	> 27.23	> 13.47
Unit tip resistance, q_{d_open} (MPa)	> 8.06	> 4.29
Plugging efficiency, η	> 0.84	> 0.29

Momiyama et al (1992) carried out a static load test on an open-ended SPP with D_o = 2000 mm having an embedment length of $8.8D_o$ into a bearing stratum having N = 40 in Tokyo Bay area. Plugging efficiency η = 0.40 was estimated at the ultimate tip resistance.

The load test results in this paper shows that use of double-crossed steel ribs (#-shaped ribs) are effective and economical way for increasing plugging efficiency of large diameter SPPs, resulting in shorter embedment lengths.

3 CONCLUDING REMARK

RLTs using a Hybridnamic device were carried out on two tests SPPs having different embedment lengths into the same bearing stratum. Double crossed steel ribs (#-shaped ribs) were attached inside the pile tip sections of a length of $2.5D_o$ to increase plugging efficiency.

The test results showed that use of double-crossed steel ribs is effective and economical way for increasing plugging efficiency of large diameter SPPs, resulting in shorter embedment lengths.

Distributions of shaft resistance were also estimated from the RLTs and were compared with empirical values specified in design code. It not only shows that the

empirical equation estimates the f_s reasonably, but also shows the importance of implementation of load tests in site for proper design piles.

Based on the load test results, SPP having shorter embedment length was adopted for the working piles of Jacket foundation for Tokyo International Cruise Terminal.

REFERENCES

1) Japanese Geotechnical Society (JGS) (2002): JGS 1815-2002 Method for Rapid Load Test of Single Piles.

2) Kamei, S., Takano, K. and Fujita, T. (2022): Comparison of static load test and rapid load test on steel pipe piles in two sites. *Proc. of the 11th International Stress Wave Conference on Stress Wave Theory and Design and Testing Methods for Dep Foundations*, Rotterdam, The Netherlands (to be published).

3) Momiyama, Y., Honma, M., Katayama, T. and Maruyama, T. (1992): Vertical Loading Test on Large-Diameter Steel-Pipe Piles for Trans-Tokyo Bay Highway, *Soil mechanics and foundation engineering*, Japanese Geotechnical Society, 40(2), 47-52 (in Japanese).

4) Ports and Harbours Bureau, Ministry of Land, Infrastructure, Transport and Tourism (MLIT) (2020): Technical Standards and Commentaries for Port and Harbour Facilities in Japan (An abridged version by The Overseas Coastal Area Development Institute of Japan, https://ocdi.or.jp/en/).

5) Raushe, F., Goble, G. and Likins, G. E., Jr. (1985): Dynamic determination of pile capacity. *ASCE Jour. Geotech. Div.*, 111(3). 367-383.

APPENDIX: ULPC method (Kamei et al., 2022)

In the ULP interpretation method, the pile is assumed to be a rigid body having a mass m supported by a nonlinear spring K and a linear dashpot as shown in Fig. A1. The load on the pile F_{rapid} is resisted by the inertia of the pile R_a, velocity-dependent resistance R_v and the static soil resistance R_w (Eq. (A1)). The soil resistance R_{soil} is obtained from Eq. (A2), using the measured F_{rapid} and α, and R_{soil} vs w is constructed as shown in Fig. A2. The static resistance R_w is then obtained using Eq. (A3), if the damping constant C is determined. The R_{soil} at the maximum displacement point (ULP) is equal to the static resistance R_w because the pile velocity v is regarded as zero at ULP (Eq. (A4) and Fig. A2).

When the Hybridnamic test is employed, generally 5 to 7 blows are applied to the pile increasing the fall height of hammer h. Hence, several values of R_{ULP} at different displacements w are obtained without determining the value of C because the pile velocity v is zero at ULP, and R_w vs w ("static" load-displacement curve) is easily obtained by connecting ULPs. This method is named Unloading Point Connection method (ULPC method).

This aspect is one of big advantages of the Hybridnamic test.

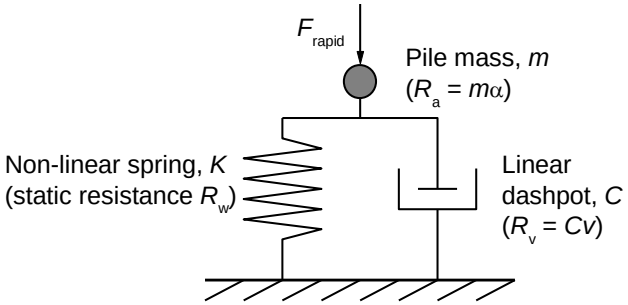

Fig. A1. Modeling of pile and soil during RLT (after Middendorp et al, 1993, and Kusakabe and Matsumoto, 1995).

$$F_{rapid} = R_a + R_v + R_w = m\,\alpha + C\,v + R_w \quad \text{(A1)}$$

$$R_{soil} = F_{rapid} - m\alpha \quad \text{(A2)}$$

$$R_w = R_{soil} - Cv \quad \text{(A3)}$$

$$R_{soil\ at\ ULP} = R_{ULP} = R_w \quad \text{(A4)}$$

where, F_{rapid} = Rapid load, R_a = Inertial force of pile, R_v = Dynamic resistance component of soil, R_w = Static resistance component, m = Pile mass, α = Pile acceleration, C = Damping constant, v = Pile velocity and R_{ULP} = ULP resistance (static resistance).

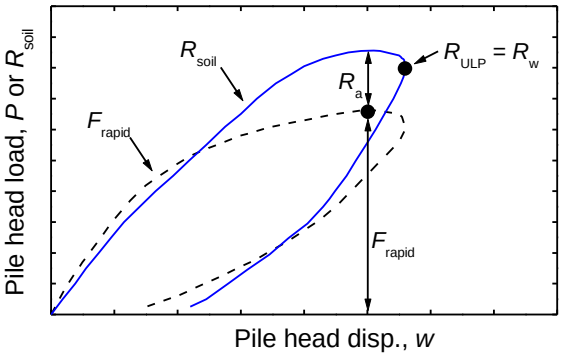

Fig. A2. Relationship between load-displacement curve and soil resistance and ULP resistance.